

Supporting Information

Shima et al. 10.1073/pnas.1217730110

SI Materials and Methods

Compounds and Cells. Kobe0065: *N*-(3-chloro-4-methylphenyl)-2-{2,6-dinitro-4-(trifluoromethyl)phenyl}hydrazinecarbothioamide, 2601: 2-(2,4-dinitrophenyl)-*N*-(4-fluorophenyl)hydrazinecarbothioamide, and 2602: 2-{2,6-dinitro-4-(trifluoromethyl)phenyl}-*N*-(4-fluorophenyl)hydrazinecarbothioamide were purchased from Namiki Shoji Co., Ltd. Sorafenib was purchased from LC Laboratories Inc. Various human cancer cell lines including SW480 were obtained from the European Collection of Cell Culture and cultured in media recommended by the supplier. *H-ras*^{G12V}- and *c-Raf-1*^{S259A/Y340D/Y341D}-transformed NIH 3T3 cells were cloned from foci obtained by focus forming assays using pT24 (1) containing the BamHI fragment of the genomic *H-ras*^{G12V} gene and pH8-flag-*c-raf-1*^{S259A/Y340D/Y341D} (2), respectively, and cultured in DMEM supplemented with 10% FBS, 100 IU/mL penicillin, and 100 μg/mL streptomycin.

Biochemical Assays. H-Ras (residues 1–166) and GST-c-Raf-1-Ras-binding domain (RBD; residues 50–131) were produced in *Escherichia coli* and purified as described previously (3, 4). For the in vitro binding inhibition assays, H-Ras(1–166), preloaded with [γ -³⁵S]GTP γ S, was incubated with GST-c-Raf-1-RBD(50–131) at 25 °C for 30 min in the presence of the compound and the amount of bound H-Ras was quantified as the radioactivity pulled down by glutathione-sepharose resin. The K_i value for the compound was calculated as described in Fig. S1. For in vivo assays, NIH 3T3 cells were transfected with pEF-BOS-HA-H-Ras^{G12V} or pEF-BOS-HA-K-Ras^{G12V}, cultured for 18 h at 10% (vol/vol) FBS, and then incubated in the presence of the compound at 2% (vol/vol) FBS for 1 h. Cells were lysed in 50 mM Tris-HCl (pH 7.4), 150 mM NaCl, 1% Nonidet P-40, 10% (vol/vol) glycerol, 1 mM EDTA, 1 mM DTT, phosphatase inhibitor mixture (Nacalai Tesque), and protease inhibitor mixture (Nacalai Tesque) and subjected to detection of c-Raf-1 coimmunoprecipitated with an anti-H-Ras antibody (C-20; Santa Cruz) by Western blotting with an anti-c-Raf-1 antibody (C-12; Santa Cruz), of phosphorylated MEK and ERK with anti-pMEK1/2 (p217/p221; Cell Signaling) and anti-ERK1/2 (p202/204; Cell Signaling) antibodies, and of phosphorylated Akt with an anti-pAkt antibody (Ser473; Cell Signaling) and of RalA-GTP pulled down with GST-Sec5(1–99) immobilized on glutathione-sepharose resin by an anti-RalA antibody (Becton Dickinson). HA-tagged H-Ras^{G12V}-GTP was detected by an anti-HA antibody (Cell Signaling). In vitro assays for the kinase activity of recombinant c-Raf-1 were performed by using a Raf-1 Kinase Assay kit (Millipore). In vitro GDP–GTP exchange assays were done by incubating 600 nM GST-H-Ras(1–166)-GDP immobilized on glutathione-sepharose resin with 11 μM [γ -³⁵S]GTP γ S (1,500 cpm/pmol) at 25 °C in the presence of purified 6×His-tagged mouse Son of sevenless (mSos)1(563–1,049) (180 nM each), wild-type, or a W729E mutant (5) in buffer B [50 mM Tris-HCl (pH 7.4), 50 mM NaCl, 5 mM MgCl₂, 1 mM DTT, and 20 mM imidazol]. The radioactivity remaining on the resin after an intensive washing was quantified by liquid scintillation counting. Varying concentrations of compounds were added to the reaction mixtures to observe their inhibitory effect.

Colony Formation Assays. Cells (10³ to 10⁴) were inoculated in 2 mL of DMEM containing 10% (vol/vol) FBS, 0.33% SeaPlaque aga-

rose, and one of the compounds and overlaid onto bottom agar consisting of 4 mL of DMEM containing 10% (vol/vol) FBS, 0.6% SeaPlaque agarose, and the same concentration of the compound in a six-well culture plate. After incubation at 37 °C for 14–21 d, the number of colonies >200 μm in diameter was counted under a dissecting microscope.

Cell Proliferation Assays. Cells (2 × 10³) were seeded in a 96-well plate and cultured in DMEM containing 2% (vol/vol) FBS in the presence of one of the compounds. Viable cell numbers were measured by formazan formation using a Cell Counting Kit 8 (Dojindo). Apoptotic cells were detected by a standard TUNEL assay using an In Situ Cell Detection kit (Roche).

Tumor Xenografts. Cells (5 × 10⁶) were implanted into the right flanks of female athymic nude mice (6–8 wk old; CLEA Japan, Inc.). After tumor sizes reached ~50 mm³ on average, compounds suspended in Cremophor:ethanol:water (1:1:6) were administered orally for five consecutive days per week for 17 d. Tumor volumes (*V*) were calculated with the following formula: $V = A \times B^2/2$, where *A* is the largest diameter and *B* is the perpendicular diameter. Dissected tumors after 17-d administration of the 80 mg/kg compounds were fixed in 4% (wt/vol) paraformaldehyde and embedded in paraffin. Their sections were subjected to immunohistochemistry with an anti-ERK1/2 antibody or an anti-CD31 antibody using a HISTMOUSE-PLUS kit (ZYMED Laboratories). Apoptotic cells were detected by a TUNEL assay. Statistical significance for groups of three or more was determined by one-way ANOVA with Tukey's test for post hoc analysis.

NMR Spectroscopy and Structure Calculation. ¹⁵N/¹³C-labeled H-Ras^{T35S}(1–166) was purified and loaded with guanosine 5'-(β , γ -imido) triphosphate as described previously (4). The NMR measurements were performed at 5 °C on an Avance III-600 spectrometer (Bruker) equipped with a 5-mm TCI cryogenic probe on a mixture of 1.0 mM H-Ras^{T35S}·GppNHp and 3.8 mM Kobe2601 in 80% ²H₂O and 20% DMSO-*d*₆. Based on assignments of the protein resonances in the absence of DMSO at 25 °C (4), 18 intermolecular distance restraints were obtained from 3D ¹³C-NOESY and 2D homonuclear NOESY spectra (mixing time 250 ms). For the structure calculation, the intraprotein distance restraints and backbone torsion angle restraints obtained in the absence of DMSO at 25 °C (4) were incorporated, assuming that the protein structure does not change upon compound binding. Among the 100 structures generated by CYANA 2.1 (6), the 20 structures with the lowest target functions were refined using CNS 1.2 (7) for selection of the lowest-energy complex structures (PDB ID code 2lwi and Table S3). The ¹H-¹⁵N HSQC spectrum of wild-type H-Ras·GppNHp were recorded on a DMX-750 spectrometer (Bruker) at 5 °C on 1.0 mM ¹⁵N-labeled H-Ras(1–166)·GppNHp in the absence or presence of 3.3 mM Kobe2601 in 90% ¹H₂O and 10% DMSO-*d*₆. Direct interactions of Kobe0065 and Kobe2602 with various small GTPases of the Ras and Rho families were examined by relaxation-edited 1D NMR (8). All of the spectra were acquired with a Carr–Purcell–Meiboom–Gill spin-lock time of 400 ms.

1. Taparowsky E, et al. (1982) Activation of the T24 bladder carcinoma transforming gene is linked to a single amino acid change. *Nature* 300(5894):762–765.

2. Tamada M, Hu CD, Kariya K, Okada T, Kataoka T (1997) Membrane recruitment of Raf-1 is not the only function of Ras in Raf-1 activation. *Oncogene* 15(24):2959–2964.

- Shima F, et al. (2010) Structural basis for conformational dynamics of GTP-bound Ras protein. *J Biol Chem* 285(29):22696–22705.
- Araki M, et al. (2011) Solution structure of the state 1 conformer of GTP-bound H-Ras protein and distinct dynamic properties between the state 1 and state 2 conformers. *J Biol Chem* 286(45):39644–39653.
- Margarit SM, et al. (2003) Structural evidence for feedback activation by Ras.GTP of the Ras-specific nucleotide exchange factor SOS. *Cell* 112(5):685–695.

- Güntert P, Mumenthaler C, Wüthrich K (1997) Torsion angle dynamics for NMR structure calculation with the new program DYANA. *J Mol Biol* 273(1):283–298.
- Brünger AT, et al. (1998) Crystallography & NMR system: A new software suite for macromolecular structure determination. *Acta Crystallogr D Biol Crystallogr* 54(Pt 5):905–921.
- Hajduk PJ, Olejniczak ET, Fesik SW (1997) One-dimensional relaxation- and diffusion-edited NMR methods for screening compounds that bind to macromolecules. *J Am Chem Soc* 119:12257–12261.

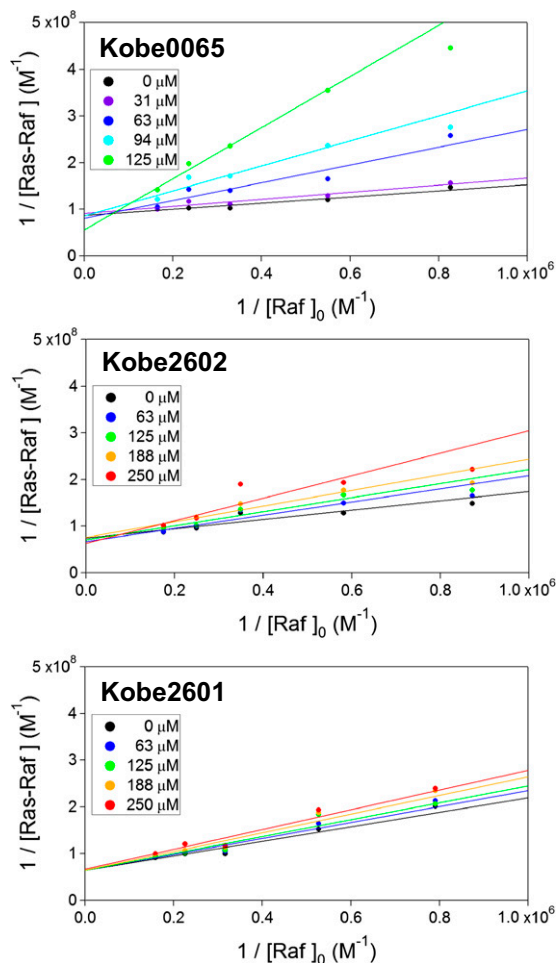
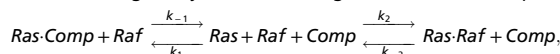


Fig. S1. Kinetic analysis of the inhibition of Ras-Raf binding by the Kobe65-family compounds. H-Ras(1–166) (0.014 μM), preloaded with $[\gamma\text{-}^{35}\text{S}]\text{GTP}\gamma\text{S}$ (1,300–1,800 cpm/pmol), was incubated with varying concentrations of GST-c-Raf-1-RBD (50–131) (0.97–6.31 μM) at 25 $^{\circ}\text{C}$ for 30 min in the presence of the indicated concentrations of the compounds in binding buffer [50 mM Tris-HCl (pH 7.4), 150 mM NaCl, 5 mM MgCl_2 , 1 mM EDTA, 0.5 mM DTT, 20% DMSO, and 0.01% Triton X-100]. The amount of bound H-Ras was quantified as the radioactivity pulled down by glutathione-sepharose resin. The double reciprocal plots of the concentrations of H-Ras bound to c-Raf-1 RBD ([Ras-Raf]) versus the initial concentrations of c-Raf-1 RBD ([Raf]₀) show that the lines obtained for different compound concentrations almost converge on the vertical axis, indicating that the compound exerts competitive inhibition against c-Raf-1 RBD. To obtain K_i values (k_{-1}/k_1) for the compounds, individual datasets were globally fitted according to a scheme of competitive inhibition as follows:



where K_d (k_{-2}/k_2) is a dissociation constant for c-Raf-1 RBD. This reaction can be formulated by the following equation:

$$\frac{1}{[\text{Ras-Raf}]} = \frac{1}{[\text{Ras}]_0} + \frac{K_d}{[\text{Ras}]_0[\text{Raf}]} \left(1 + \frac{[\text{Comp}]}{K_i} \right),$$

where $[\text{Ras}]_0$ and $[\text{Comp}]$ are the initial concentration of H-Ras-GTP γS and the compounds, respectively. The K_d value for c-Raf-1 RBD was $1.81 \pm 1.19 \mu\text{M}$ and the K_i values for Kobe0065, Kobe2602, and Kobe2601 were 46 ± 13 , 149 ± 55 , and $773 \pm 49 \mu\text{M}$, respectively, as calculated from three independent experiments.

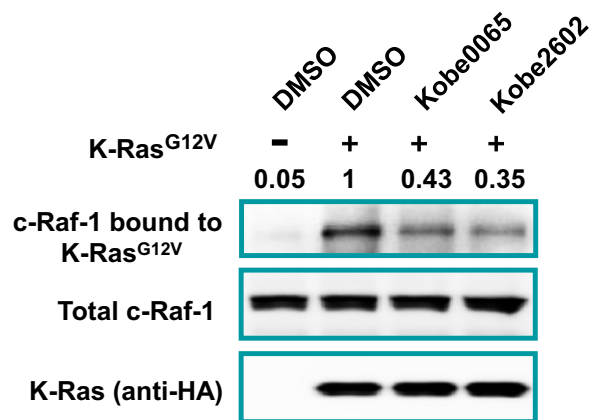


Fig. S2. Inhibition of the K-Ras^{G12V}-c-Raf-1 binding in cells by the Kobe0065-family compounds. NIH 3T3 cells were transfected with pEF-BOS-HA-K-Ras^{G12V} or an empty vector and treated with 20 μ M Kobe0065, 20 μ M Kobe2602, or the vehicle (DMSO) in the presence of 2% (vol/vol) FBS for 1 h. Cell lysate was subjected to detection of c-Raf-1 coimmunoprecipitated with K-Ras^{G12V} by an anti-HA antibody (*Top*) and total c-Raf-1 (*Middle*) by Western blotting with an anti-c-Raf-1 antibody. The numbers above the lanes show the values of K-Ras-bound/total c-Raf-1 relative to that of the vehicle-treated cells.

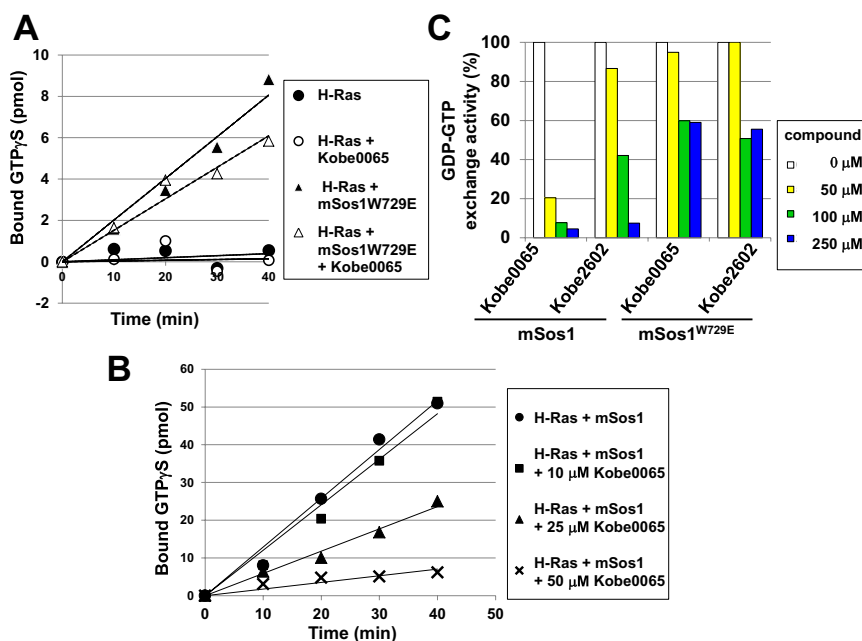


Fig. S3. Effect of the Kobe0065-family compounds on the Sos-stimulated GDP-GTP exchange. (A) Effect of Kobe0065 on the mSos1^{W729E}-stimulated nucleotide exchange. The GDP-GTP exchange activity of H-Ras dependent on mSos1^{W729E} was measured as described in the legend to Fig. 2A and compared with the intrinsic nucleotide-exchange activity of H-Ras. Three independent experiments yielded essentially equivalent results. (B) Dose-dependent inhibition of the mSos1-stimulated nucleotide exchange reaction by Kobe0065. The GDP-GTP exchange activity of H-Ras dependent on mSos1 was measured in the presence of the indicated concentrations of Kobe0065 as described above. (C) Dose-dependent inhibition of Sos-stimulated nucleotide exchange by the compounds. The nucleotide exchange activity of H-Ras dependent on mSos1 or mSos1^{W729E} was measured in the presence of the indicated concentrations of the compounds as described above.

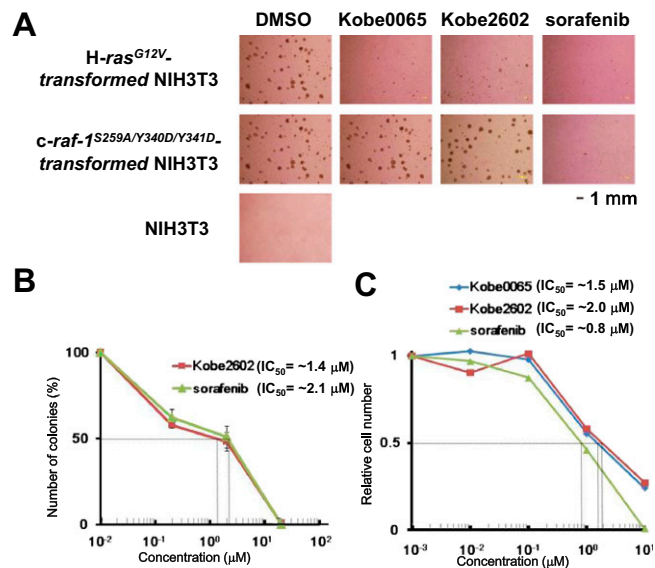


Fig. 54. Specific inhibition of anchorage-independent and -dependent growth of H-*ras*^{G12V}-transformed cells by the Kobe0065-family compounds. (A) Effects of the 20 μM compounds on soft agar colony formation of NIH 3T3 cells transformed by the H-*ras*^{G12V} and c-*raf-1*^{S259A/Y340D/Y341D} genes were examined as described in the legend to Fig. 3, A and C. A representative image is shown for each group. (B) The IC_{50} values for Kobe2602 and sorafenib on anchorage-independent growth were estimated from the corresponding dose-response curves. The values are presented as the mean \pm SEM; $n = 5-6$. (C) The IC_{50} values for Kobe0065, Kobe2602, and sorafenib on anchorage-dependent growth were estimated from the corresponding dose-response curves. Each point represents the viable cell number at 72 h of treatment relative to the initial number. Shown are representative data.

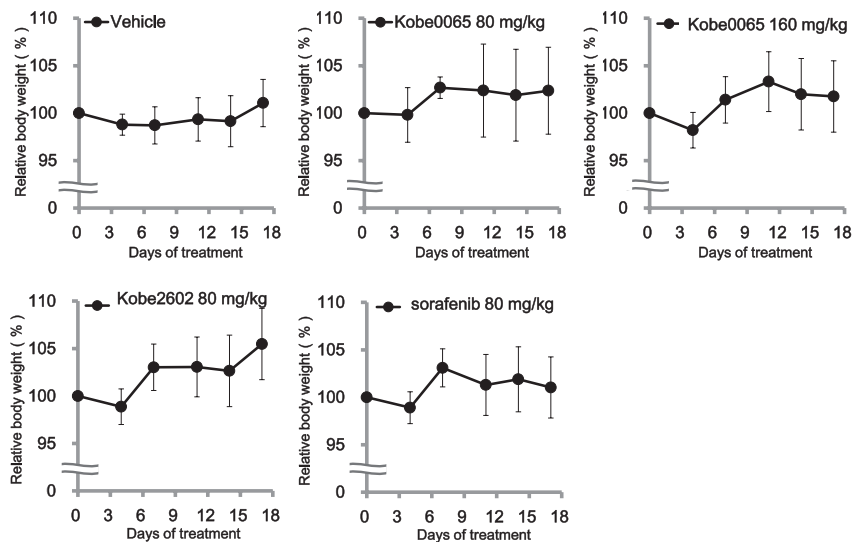


Fig. 55. No significant effect of the administration of the Kobe0065-family compounds on the mouse body weight. The body weight changes of the tumor-grafted mice, administered orally with the indicated doses of the compounds or the vehicle for 17 d (see the legend to Fig. 4A and *SI Materials and Methods*) are shown. Each point represents the mouse body weight, the mean \pm SEM; $n = 8-10$ per group, relative to that at day 0.

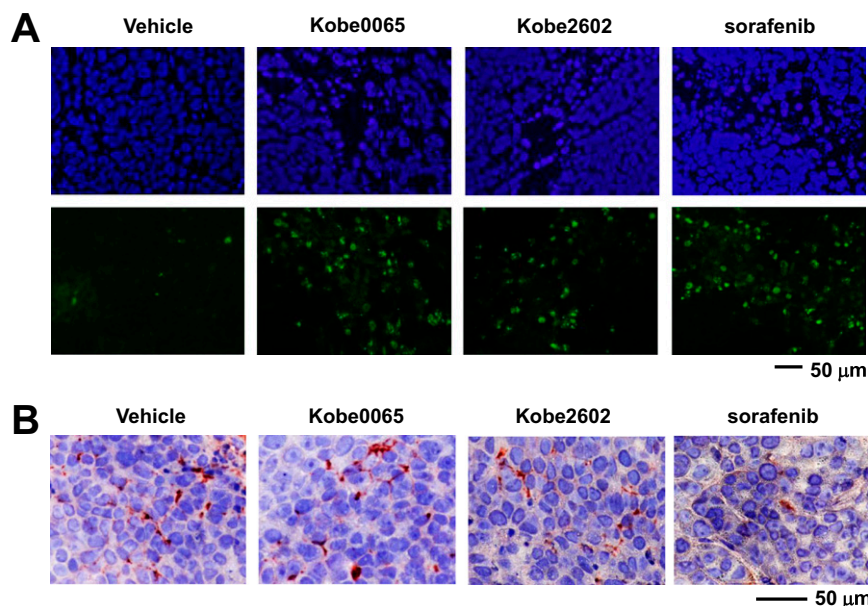


Fig. S6. Effects of the administration of the Kobe0065-family compounds on apoptosis and angiogenesis of tumors. (A) Tumors were isolated after daily treatment with the indicated compounds at 80 mg/kg or the vehicle for 17 d and their sections were subjected to staining with DAPI (*Upper*) and the TUNEL assay (*Lower*). (B) Tumor sections prepared as described in A were subjected to immunohistochemical detection of platelet endothelial cell adhesion molecule-1 with an anti-mouse CD31 antibody (BD Pharmingen). A representative image is shown for each group.

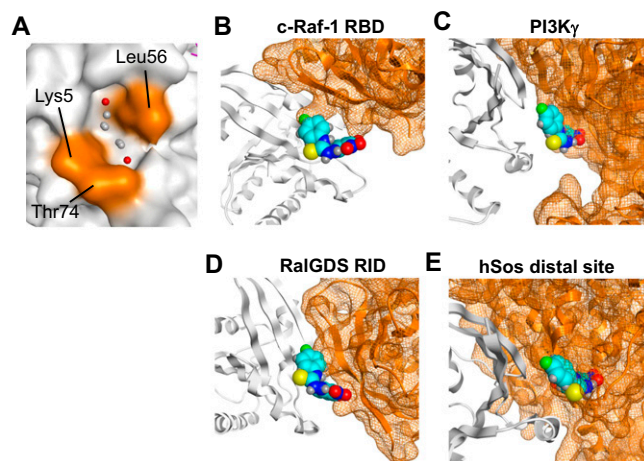


Fig. S7. Structural basis for inhibition of the Ras-effector interactions by the Kobe65-family compounds. (A) A close-up view of the Kobe2601-binding pocket in the crystal structure of H-Ras^{T355}·GppNHp (PDB ID code 3KKM) (1). The cluster of small spheres (hydrophilic, red; hydrophobic, gray) indicates a pocket identified by the Site Finder module in the Molecular Operating Environment (MOE) software package (Chemical Computing Group Inc.). (B–E) Predicted spatial configurations of Kobe2601 in various Ras-effector complexes. The NMR structure of the H-Ras^{T355}·GppNHp–Kobe2601 complex with the lowest energy target function was superimposed on the Ras or Rap1 molecule in the crystal structures of the Rap1A·GppNHp–c-Raf-1 RBD complex (PDB ID code 1C1Y) (B), H-Ras^{G12V}·GppNHp–PI3K γ complex (PDB ID code 1H8E) (C), H-Ras^{E31K}·GppNHp–RalGDS RID complex (PDB code ID 1LFD) (D), and H-Ras^{Y64A}·GppNHp–hSos complex (PDB ID code 1NVV) (E), by fitting to minimize root mean square deviations for the residues 1–31, 39–59, and 76–166, followed by removal of the Ras or Rap1 molecule. H-Ras^{T355} and the effectors are colored in white and brown, respectively. Kobe2601 is represented by a space-filling model. The fitting and molecular visualization were carried out using the MOE software package.

1. Shima F, et al. (2010) Structural basis for conformational dynamics of GTP-bound Ras protein. *J Biol Chem* 285(29):22696–22705.

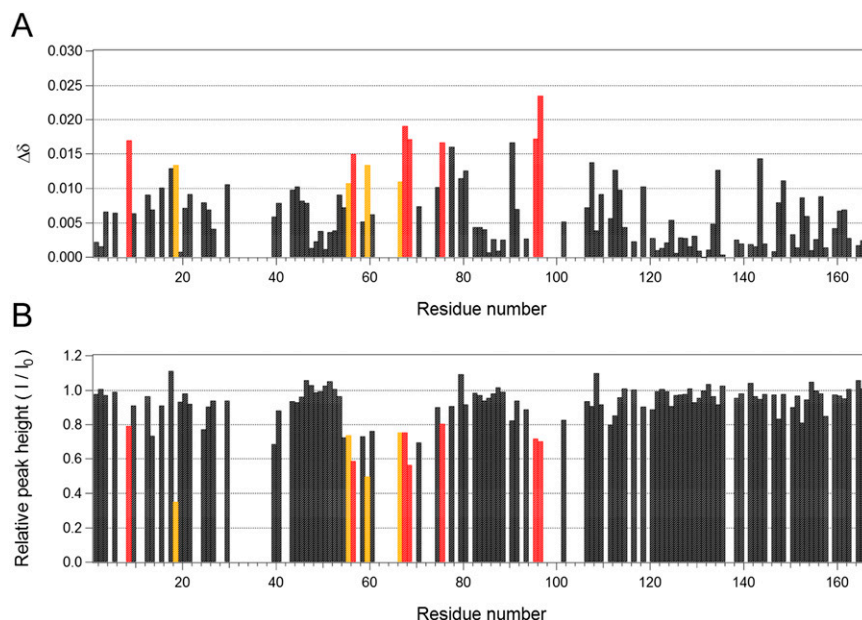


Fig. 58. Mapping of the residues of wild-type H-Ras-GppNHp involved in compound interaction by ^1H - ^{15}N HSQC spectroscopy. (A) Plot of the weighted averages of the backbone ^1H and ^{15}N chemical shift changes, calculated by using the function: $\Delta\delta = [(\Delta\delta_{1\text{H}})^2 + 0.01(\Delta\delta_{15\text{N}})^2]^{0.5}$ against the residue numbers. Data are missing for three proline residues, some switch region residues whose signals could not be assigned, and some residues whose signals showed overlaps with others. (B) Plot of the peak heights in the presence of Kobe2601 against the residue numbers. Each peak height (I) was normalized relative to that in the absence of the compound (I_0). In the case of the residues that exhibit cross-peak splitting (1), averaged $\Delta\delta$ and I/I_0 values are presented. The perturbed residues with $0.01 \leq \Delta\delta < 0.015$ and $I/I_0 \leq 0.8$, orange; $\Delta\delta \geq 0.015$ and $I/I_0 \leq 0.8$, red. The spectrum in the absence or presence of Kobe2601 was acquired with 2,048 complex points covering 10,000 Hz for ^1H and 256 complex points covering 4,000 Hz for ^{15}N and analyzed using Sparky (University of California, San Francisco).

1. Araki M, et al. (2011) Solution structure of the state 1 conformer of GTP-bound H-Ras protein and distinct dynamic properties between the state 1 and state 2 conformers. *J Biol Chem* 286(45):39644–39653.

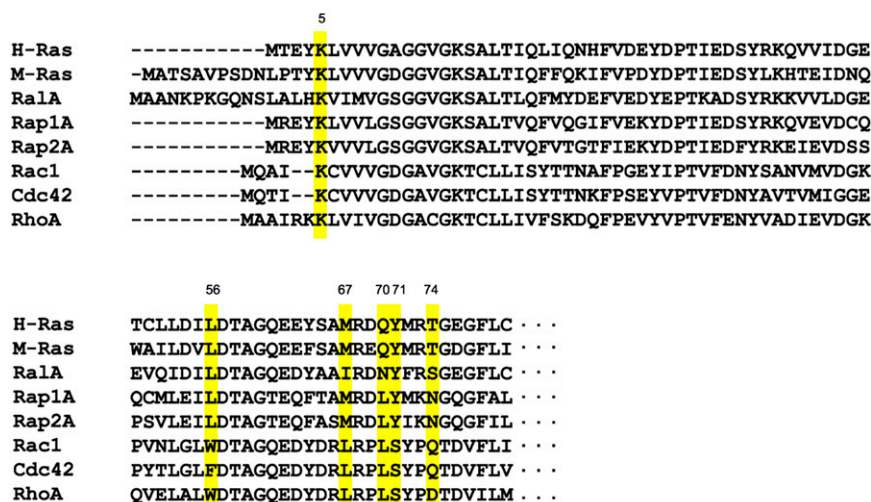


Fig. 59. Sequence comparison of the residues involved in interaction with Kobe2601 in H-Ras. The amino acid sequences of the residues that exhibit NOE contacts with Kobe2601 and form a hydrophobic surface pocket in H-Ras^{T35S}.GppNHp are conserved among various small GTPases of the Ras and Rho families, as highlighted in yellow. Multiple sequence alignments were generated using the program ClustalX (1).

1. Larkin MA, et al. (2007) Clustal W and Clustal X version 2.0. *Bioinformatics* 23(21):2947–2948.

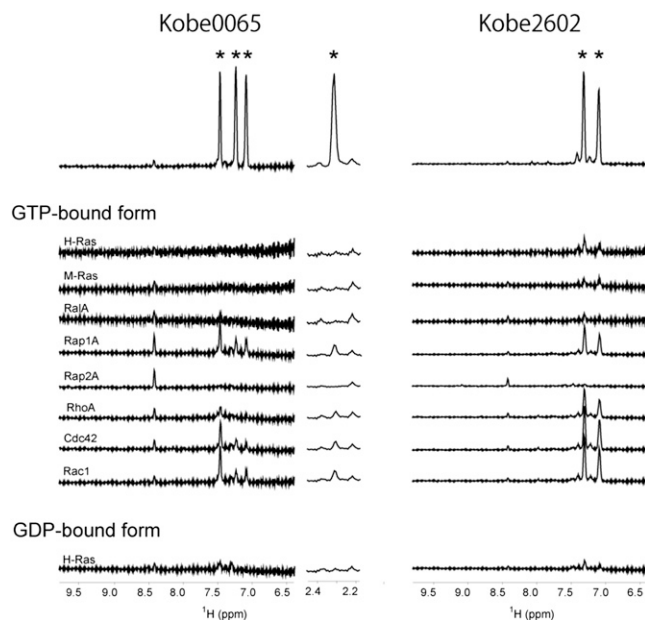


Fig. S10. Relaxation-edited 1D ^1H NMR analysis of the interaction of the Kobe0065-family compounds with various small GTPases. Human H-Ras(1–166) and mouse M-Ras(1–178), human RhoA, human Rac1, and human Cdc42 were expressed as GST fusions in *Escherichia coli* using pGEX-6P-1 vector (GE Healthcare), immobilized on glutathione-sepharose resin, and eluted by cleavage with PreScission protease (GE Healthcare) as described previously (1, 2). Human RalA, human Rap1A(1–167), and human Rap2A were expressed with an N-terminal 6xHis tag and affinity-purified as described previously (2). The purified H-Ras was used as the GDP-bound form. Otherwise, the small GTPases were loaded with GppNHp as described previously (2). Direct interaction of Kobe0065 and Kobe2602 with the small GTPases were analyzed at a compound:protein molar ratio of 1:3 by relaxation-edited 1D NMR (3). Kobe2601 could not be used because it underwent a chemical exchange resulting in significant signal attenuation. All of the spectra were acquired with a Carr–Purcell–Meiboom–Gill spin-lock time of 400 ms. The compound-specific signals in the spectra (Upper), indicated by asterisks, show line broadening and height reduction and eventually disappear when the compound binds directly to the small GTPases. The residual signal at 8.4 ppm was derived from an impurity in the sample buffer.

1. Shima F, et al. (2010) Structural basis for conformational dynamics of GTP-bound Ras protein. *J Biol Chem* 285(29):22696–22705.
2. Liao J, et al. (2008) Two conformational states of Ras GTPase exhibit differential GTP-binding kinetics. *Biochem Biophys Res Commun* 369(2):327–332.
3. Hajduk PJ, Olejniczak ET, Fesik SW (1997) One-dimensional relaxation- and diffusion-edited NMR methods for screening compounds that bind to macromolecules. *J Am Chem Soc* 119: 12257–12261.

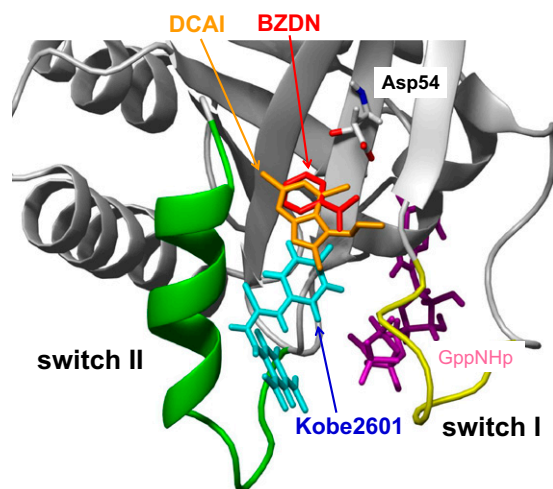


Fig. S11. Comparison of the spatial configurations of Kobe2601 with other Ras inhibitors in the H-Ras^{T355}-GppNHp structure. The NMR structure of the H-Ras^{T355}-GppNHp–Kobe2601 complex with the lowest-energy target function was superimposed on K-RasG12D-GTPγS–BZDN (PDB ID code 4DSO) and K-RasG12D-GppCHp–DCAI (PDB ID code 4DST) (1) using the backbone atoms of the residues 1–31, 39–59, and 76–166. The arrangements of benzamidine (BZDN, orange) and 4,6-dichloro-2-methyl-3-aminoethyl-indole (DCAI, red) are shown on the backbone structure of the H-Ras^{T355}-GppNHp–Kobe2601 complex.

1. Maurer T, et al. (2012) Small-molecule ligands bind to a distinct pocket in Ras and inhibit SOS-mediated nucleotide exchange activity. *Proc Natl Acad Sci USA* 109(14):5299–5304.

Table S1. Effect of the Kobe0065-family compounds on the anchorage-independent growth of various human cancer cells

Cell line	Organ	H-Ras	K-Ras	N-Ras	B-Raf	PTEN	PIK3CA	Inhibitory effect, %		
								Kobe0065	Kobe2602	Sorafenib
SW480	Colon		G12V					66.30	65.00	83.80
PANC-1	Pancreas		G12D					63.50	96.00	96.30
EJ-1	Bladder	G12V						62.70	51.50	87.70
HT1080	Tissue			Q61L				79.00	80.50	70.00
DLD-1	Colon		G13D				E545K	60.50	63.00	80.70
HCT116	Colon		G13D				H1047R	55.00	59.00	99.00
A375	Melanoma				V600E			26.00	41.00	93.00
T-47D	Breast						H1047R	11.00	25.00	97.00
LNCap	Prostate					Frameshift		49.00	23.00	87.00
BxPC-3	Pancreas							15.00	24.00	59.70
MCF-7	Breast						E545K	26.00	27.00	93.00
HepG2	Liver							14.50	0	72.50
HeLa	Cervix							13.50	23.50	86.90

Experiments were performed three times, and each experiment used two wells per compound. PIK3CA, phosphatidylinositol-4,5-; PTEN, phosphatase and tensin homolog.

Table S2. Structural statistics for the 15 lowest energy structures of the H-Ras^{T35S}•GppNHp-Kobe2601 complex

Number of distance restraints	
Total	3138
Intramolecular NOEs (H-RasT35S•GppNHp)	
Intraresidue	815
Short-range ($ i-j = 1$ residue)	749
Medium-range ($ i-j = 2$ to 4 residues)	532
Long-range ($ i-j > 4$ residues)	1023
Intermolecular NOEs	19
Number of torsion angle restraints	
ϕ/ψ	114/116
RMSD from experimental restraints	
Distance constraints (Å)	0.0075 ± 0.0009
Torsion angle constraints (°)	0.045 ± 0.029
RMSD from ideal covalent geometry	
Bond lengths (Å)	0.0011 ± 0.0001
Bond angles (°)	0.34 ± 0.01
Improper (°)	0.29 ± 0.03
RMSD from the mean structure (Å)	
Backbone atoms (residues 1–27, 39–59, 76–166)	0.43 ± 0.06
All heavy atoms (residues 1–27, 39–59, 76–166)	0.83 ± 0.06
Backbone atoms (residues 1–166)	0.78 ± 0.19
All heavy atoms (residues 1–166)	1.21 ± 0.19
Ramachandran analysis	
Most favored regions (%)	82.0
Additional allowed regions (%)	15.5
Generously allowed regions (%)	2.2
Disallowed regions (%)	0.3

Ramachandran analysis was evaluated by the program PROCHECK (1).

1. Laskowski RA, Rullmann JA, MacArthur MW, Kaptein R, Thornton JM (1996) AQUA and PROCHECK-NMR: programs for checking the quality of protein structures solved by NMR. *J Biomol NMR* 8(4):477–486.

